European Journal of Pharmaceutics and Biopharmaceutics 71 (2009) 88–99

Contents lists available at ScienceDirect

European Journal of Pharmaceutics and Biopharmaceutics

journal homepage: www.elsevier.com/locate/ejpb

Research paper

The study of different solid forms of Emodepside

Julia Baronsky [a,b,*], Sabine Bongaerts [b], Michael Traeubel [b], Hans-Christoph Weiss [c], Nora Urbanetz [a]

[a] Institute of Pharmaceutics and Biopharmaceutics, Heinrich-Heine-University, Duesseldorf, Germany
[b] BHC-AH-RD-A, Bayer HealthCare AG, Leverkusen, Germany
[c] CUR-SER-ANT, Currenta GmbH & Co. OHG, Leverkusen, Germany

ARTICLE INFO

Article history:
Received 18 January 2008
Accepted in revised form 9 June 2008
Available online 17 June 2008

Keywords:
Non-stoichiometric hydrates
Isomorphic dehydrates
Crystal structure
Thermal analysis
Vapour sorption
NIR spectroscopy
Raman spectroscopy

ABSTRACT

Emodepside is an endoparasiticide used in veterinary drugs. It exists in four different crystal forms which were characterised using DSC, TGA, evolved gas analysis (using FT-IR spectroscopy), hot-stage microscopy, FT-Raman, FT-IR and FT-NIR spectroscopy and powder X-ray diffraction. Thermal analysis showed that the forms II–IV contain considerable amounts of water being easily lost upon heating. Hot-stage microscopy indicated that the crystal structures do not change upon the loss of water. To examine whether the forms II–IV are hydrates or modifications of Emodepside having water adsorbed to the crystal surface and/or absorbed into disordered defect regions, the behaviour of the forms at different relative humidities was analysed using FT-Raman and FT-NIR spectroscopy and vapour sorption analysis. Changes in the C=O stretching region in the Raman spectra upon the removal of water revealed that all three forms represent non-stoichiometric hydrates forming isomorphic dehydrates. Sorption analysis indicated the presence of localised water molecules in the structure of form IV. Several OH combination bands of water were found in the NIR spectrum of each form indicating differently bound water molecules. Crystal structure analysis of form IV at ambient humidity revealed four well-defined water positions in the asymmetric unit.

1. Introduction

Hydrates are found among antibiotics, antiphlogistic drugs, local anaesthetics, antiasthmatic drugs and other groups of pharmacologicals [1–4]. As water is omnipresent, the possibility of hydrate formation has to be taken into consideration at each step of drug development [5]. In the case of having a crystalline active pharmaceutical ingredient (API) which exists in several crystal forms one of which is associated with water, it is important to elucidate whether this form is a solid two component system in which water molecules are incorporated into the crystal lattice of the API (hydrate) or whether it is a crystal modification of the API having water adsorbed to the crystal surface and/or absorbed into disordered defect regions (“wet bulk”). If the latter is the case, the thermodynamic relationship between this form and the other crystal modifications of the API can be predicted. However, in case the form is a hydrate, it is regarded as an individual compound and no thermodynamic relationship can be established.

Hydrates are of complex nature due to the various possibilities of incorporation of the water molecules into the crystal lattice [6]. One possibility to classify hydrates is the division into stoichiometric and non-stoichiometric hydrates [7]. Stoichiometric hydrates have a fixed amount of water inside the crystal lattice. In contrast, non-stoichiometric hydrates incorporate water molecules into the crystal lattice in dependence on the water activity of the surrounding atmosphere without changing the packing motif of the crystal [8].

In non-stoichiometric hydrates, the water molecules fill structural voids present in the crystal structure [9]. These voids are connected to form tunnels through which the water molecules can enter and leave the solid. The water molecules incorporated are either ordered occupying fixed positions in the crystal lattice or they are disordered moving easily from one bonding position to the other [7]. Upon the desorption of the last water molecules, some non-stoichiometric hydrates such as cromolyn sodium turn into an amorphous state [7,10] while others, e.g. erythromycin A dihydrate, dehydrate retaining their crystal structure [11,12].

Non-stoichiometric hydrates that form isomorphic dehydrates (also called dehydrated hydrates) might be challenging to identify due to the fact that dehydration causes only subtle changes to the crystal lattice [13,14]. If crystal structure determination is possible, it is a powerful tool to identify this type of hydrate [9]. Other methods employed to identify such hydrates are powder X-ray diffraction (PXRD) and solid-state NMR [11,15]. PXRD detects anisotropic shrinking of the crystal lattice which usually takes place upon dehydration. This reduction in the unit cell volume

* Corresponding author. Bayer HealthCare AG, BHC-AH-RD-A, Building 6820, 51368 Leverkusen, Germany. Tel.: +49 21 73 38 46 80; fax: +49 21 73 38 30 27.
E-mail address: julia.baronsky@bayerhealthcare.com (J. Baronsky).

0939-6411/$ - see front matter © 2008 Elsevier B.V. All rights reserved.
doi:10.1016/j.ejpb.2008.06.003

leads to small shifts of peaks in the X-ray diffraction pattern towards smaller d spacings, shown for example for the dehydrates of cephalexin monohydrate and erythromycin A dihydrate [11]. Solid-state NMR, in contrast, is sensitive to small changes in the local chemical environment caused by the leaving of the water molecules [9,15].

However, in case the crystal structure is not known and the powder X-ray diffractogram does not exhibit any changes upon the removal of water (as the positions of the peaks do not necessarily have to shift [11]), the proof that the examined substance represents a hydrate is not straightforward. Additionally, since it is common for non-stoichiometric hydrates to show an early and continuous loss of water when analysed with TGA and moisture sorption and desorption curves with little hysteresis [1,11], the data might be misinterpreted and the solid might be regarded as single component system with water adsorbed to the crystal surface.

Emodepside, an endoparasiticide used in veterinary drugs, represents such a case where the question comes up whether hydrates or modifications with water adsorbed to the crystal surface and/or absorbed into disordered defect regions are present. Emodepside, a cyclooctadepsipeptide (Fig. 1), exists in at least four different crystal forms. These four forms were investigated using DSC, TGA, evolved gas analysis (the gases evolved during the heating of the sample were analysed using FT-IR spectroscopy), hot-stage microscopy, FT-Raman spectroscopy, FT-IR spectroscopy, FT-NIR spectroscopy and powder X-ray diffraction. DSC, TGA and evolved gas analysis revealed the forms II–IV to be associated with considerable amounts of water at ambient conditions which are readily lost upon heating. Hot-stage microscopy did not indicate a change of the crystal structures of the forms II–IV upon the loss of water.

The aims of this study are (1) to elucidate whether the forms II–IV are hydrates and if this is the case, (2) to gain information on how the water molecules are incorporated into the crystal lattice. The behaviour of the different forms at varying RH was examined using FT-Raman and FT-NIR spectroscopy and water vapour sorption analysis. As Raman analysis is sensitive to changes of intermolecular bonding inside the crystal lattice, it has been shown to be suitable to differentiate between hydrate and isomorphic dehydrate [16]. NIR spectroscopy has been used to obtain information on the bonding status of the water molecules in hydrates [17]. The sensitivity to water (as a molecule with hydrogen to heteroatom bonds) and the higher penetration depth of light compared to mid IR make NIR spectroscopy a valuable tool to gain information on the environment of the water molecules in the crystal lattice [18]. Regarding form IV, crystal structure determination was performed and the obtained crystal structure was compared to the results gained from the combination of Raman, NIR and vapour sorption analysis.

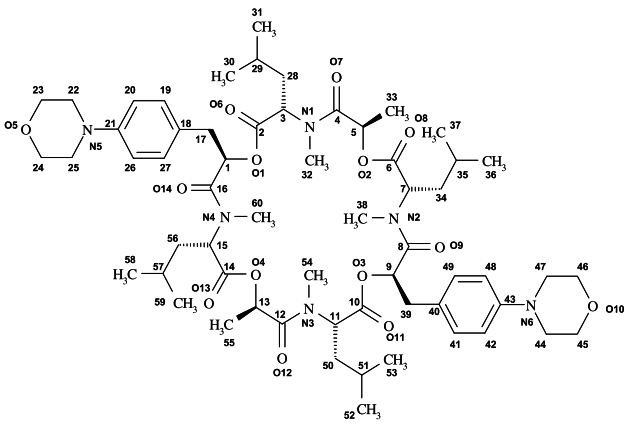

Fig. 1. Molecular structure and numbering scheme of Emodepside.

2. Materials and methods

2.1. Materials

All solvents used were of analytical grade. The forms I and II of Emodepside were available from batches of industrial production. Form II was additionally produced in laboratory scale. The preparation of the forms III and IV was performed in laboratory scale.

2.2. Preparation of crystal forms and storage

Emodepside form I (batch of industrial production) was prepared by adding a hot ethyl acetate solution (45–55 °C) to hot diisopropyl ether (65–75 °C).

Form II (batch of industrial production) was formed when adding diisoproyl ether dropwise to a hot ethanol solution (65 °C). In laboratory scale, a boiling solution (near saturation) of Emodepside in ethanol 96% was filtered and cooled at room temperature to obtain crystals of form II.

Form III crystallised from acetone as well as from isopropanol. It was prepared by either cooling a boiling acetone or isopropanol solution (near saturation) at room temperature or by slurry phase conversion. For the latter method, form II of Emodepside was suspended in either acetone or isopropanol at room temperature and stirred at least overnight.

Form IV was formed by suspending form II of Emodepside in methanol at room temperature and stirring the suspension overnight. Additionally, form IV was prepared by cooling a boiling methanol solution at room temperature. Single crystals of form IV were obtained by cooling a boiling methanol solution of Emodepside (2% (m/V)) at room temperature in a round-bottomed flask.

The crystals of the forms II–IV produced in laboratory scale were dried in vacuo at 45 °C overnight.

All forms of Emodepside were stored at ambient conditions (45% RH ± 15% RH) unless otherwise stated until further required.

2.3. Thermal analysis

2.3.1. Hot-stage microscopy

Microscopic investigations were performed using a Thermovar polarising light microscope (Leica Biosystems Nussloch GmbH, Wetzlar, Germany) equipped with a hot-stage. The samples were examined with crossed polarisers, first at room temperature and then at 120 °C.

2.3.2. Differential scanning calorimetry (DSC)

DSC curves were recorded with a DSC 822e instrument (Mettler Toledo GmbH, Giessen, Germany). About 3–7 mg of the sample was weighed into an aluminium pan and sealed with a perforated lid. The samples were heated with 10 °C/min under a nitrogen purge of 50 ml/min from 25 to 230 °C. Before, the system had been calibrated under the same conditions using indium.

2.3.3. Thermogravimetry (TGA)

To monitor the mass change of the sample, a TG system (Mettler Toledo GmbH, Giessen, Germany) equipped with a TGA850 thermobalance was used. The samples were heated from 25 to 230 °C with 10 °C/min in an open aluminium pan while nitrogen was passed along the open pan (50 ml/min) as well as along the balance (10 ml/min). Prior to measurements, the temperature had been calibrated using indium and aluminium.

2.4. FT-Raman spectroscopy

Each form of Emodepside was measured without further preparation to obtain the spectra of the different forms at ambient conditions. To examine how the spectra behave at low and high RH, respectively, samples of each form were stored at 22 °C over phosphorus pentoxide (0% RH) and over a saturated aqueous potassium chloride solution (85% RH) for 7 days before measurement (using exsiccators). To minimise the time the conditioned samples were exposed to ambient humidity before recording started, the samples were equilibrated in the sample holders (glass vials) which were sealed immediately after they had been taken out of the exsiccators. Raman spectra were acquired with a Bruker RFS 100S spectrometer (Bruker Optik GmbH, Ettlingen, Germany) using a Nd:YAG laser (1064 nm) as excitation source and a high sensitivity Ge-detector (cooled with liquid nitrogen). The spectra were recorded from 3500 to 20 cm^{-1} at a resolution of 1 cm^{-1} (128 scans) using a laser output of 750 mW. Before comparing the spectra of each form obtained at different RH, the spectra were normalised using the standard normal variate (SNV) method over the range of 3200–570 cm^{-1}. The region below 570 cm^{-1} was excluded from normalisation because of the presence of spectral features (baseline drift and a single, very intense and sharp band at around 84 cm^{-1}) that would impair the result of SNV normalisation if included into the spectral data range being treated with SNV.

2.5. FT-IR spectroscopy

Infrared analysis was carried out with a FT-IR Bruker Tensor 37 spectrometer (Bruker Optik GmbH, Ettlingen, Germany). ATR was used as sampling method. Spectra were recorded over the range of 4000–550 cm^{-1} at a resolution of 2 cm^{-1} (64 scans).

2.6. FT-NIR spectroscopy

The spectra at ambient conditions were obtained without further preparation of the samples. To minimise scatter effects, the spectra were treated with SNV. To acquire spectra at different RH, samples of each form of Emodepside were stored at 22 °C in exsiccators either containing phosphorus pentoxide (0% RH) or a saturated aqueous solution of lithium chloride (11% RH), potassium thiocyanate (47% RH), ammonium nitrate (62% RH) or potassium chloride (85% RH) prior to measurement. After a storage period of 7 days, NIR spectra were recorded on a Bruker IFS 28N spectrometer (Bruker Optik GmbH, Ettlingen, Germany) equipped with a fibre optic probe. The scanned wavelength range was 1000–2500 nm at a resolution of 8 cm^{-1} (15 scans). To compare the spectra obtained at different RH, the second derivative of the raw spectra was produced.

2.7. Powder X-ray diffraction (PXRD)

Powder X-ray diffraction was performed on a STOE STADI-P transmission diffractometer (STOE & Cie GmbH, Darmstadt, Germany) using CuKα_1 radiation, a voltage of 45 kV and a current of 35 mA. Data were collected over the range of 2–38° (2θ) at a scan rate of 310 s per step and a step size of 0.01° (2θ) using a linear Position Sensitive Detector.

2.8. Water vapour sorption/desorption analysis

Sorption/desorption isotherms were recorded using an in-house temperature and humidity controlled moisture balance at 22 °C. After the insertion of the samples, the system was evacuated and the samples were dried for 140 h. The desired RH was then set by allowing the influx of the appropriate amount of water vapour. The RH was increased from 0% RH to 90% RH in 10% steps using 3% RH, 6% RH, 15% RH and 95% RH as additional steps (sorption isotherm). To obtain the desorption isotherm, the RH was decreased to 85% RH first and then lowered from 85% RH to 10% RH in 15% steps. Finally, the RH was reduced to 6% RH, 4% RH, 2% RH and 0% RH. The absolute value of the rate of change in mass had to be $\leq$2 ppm/h before the RH was changed to the next step.

2.9. Crystal structure determination

Crystal structure determination was carried out using a Xcalibur diffractometer (Oxford diffraction Ltd., Abingdon, United Kingdom) equipped with CuK radiation (λ = 1.54178 Å), a Cryojet low temperature device (T = 100 K) and a CCD area detector (model Ruby). Crystal structure solution was achieved using direct methods as implemented in SHELXTL [19]. Least-squares refinement on F2 using all measured intensities was carried out using SHELXTL [19].

3. Results and discussion

3.1. Thermal analysis

3.1.1. DSC and TGA

The DSC measurements are shown in Fig. 2. Form I shows a single endothermic peak representing the melting of form I. The forms II–IV however exhibit two endothermic events. The first takes place below 100 °C having a broad shape. The endotherm is accompanied by a weight loss as revealed by thermogravimetric analysis (Fig. 2). Evolved gas analysis using FT-IR spectroscopy (data not presented) shows that the weight loss is due to the evaporation of water. The second endotherm represents the melting of the water-free forms of II, III and IV. Regarding the forms III and IV, shape and position of the melting peak may vary from batch to batch depending on the crystallisation process used. The batches of both forms showing a lower and broad melting endotherm (IIIA and IVA) were obtained by slurry phase conversion at room temperature. The suspensions were stirred overnight and filtered the next day. Photomicrographs of IIIA and IVA (Fig. 3) display agglomerates of small crystals. The not uniformly melting batch of form IV (IVB) was produced by cooling a hot methanol solution at room temperature, whereas the batch of form III showing the split peak (IIIB) was obtained analogous to IIIA, however, the solid was left in its mother liquor for 12 days before filtration. Photomicrographs of IIIB and IVB (Fig. 3) reveal that the batches represent mixtures of small crystals and crystals which are considerably bigger than the crystals present in IIIA and IVA. These big crystals are shaped like needles (IVB) and blades (IIIB), respectively. Contrarily to the differences in the DSC curves and in the microscopical appearances of the crystals, the different batches of form III (IV) display identical IR, Raman, NIR spectra and TGA curves confirming that they represent the same crystal form at room temperature. To examine whether the non-uniform shape of the second endotherm of IIIB and IVB might correspond to several events taking place (e.g. melting – crystallisation – melting), hot-stage microscopy and variable temperature FT-IR spectroscopy were performed (not shown). However, measurements suggest just the melting of the batches. Additionally, degradation of the substance was ruled out after having examined the molten batches using HPLC. The differences in the melting behaviour might be explained by the differences in the crystal size and by the shapes of the crystals present in IIIB and IVB. Small crystals that agglomerate show better heat conduction thus melting at lower temperature than big needles or blades which have lower bulk densities and show only punctual contact. Therefore, the batches IIIB and IVB having both small crystals and big needles or blades exhibit a non-uniform melting peak.

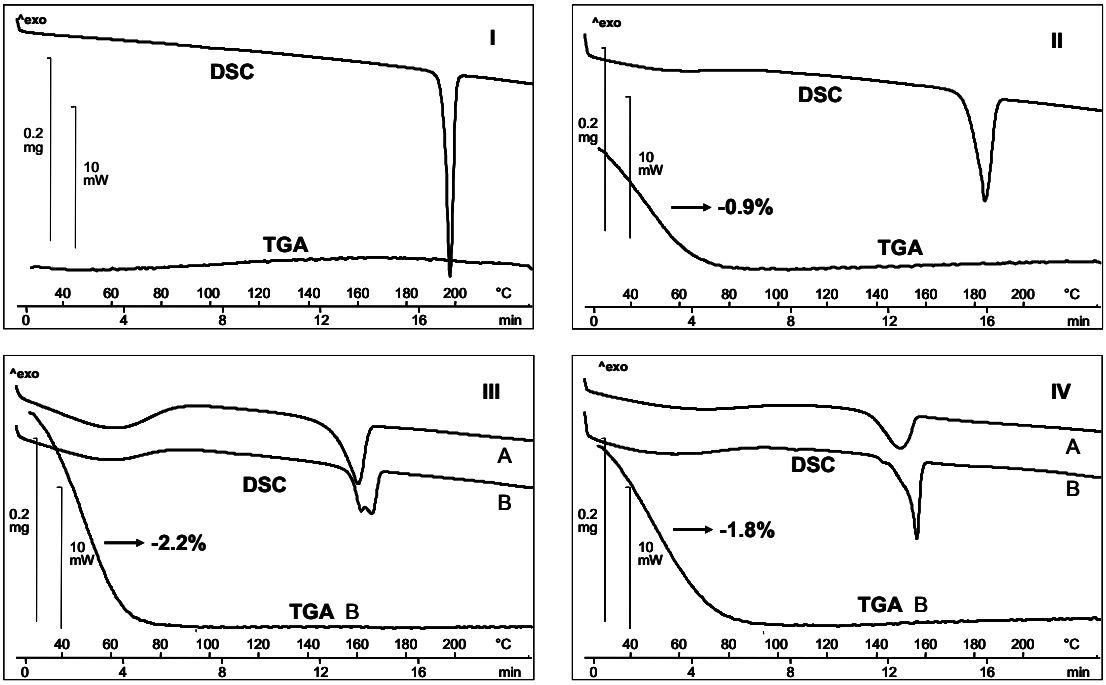

Fig. 2. The DSC and the TGA curves of the forms I–IV of Emodepside. IIIA and IIIB as well as IVA and IVB represent different batches obtained from different crystallisation procedures.

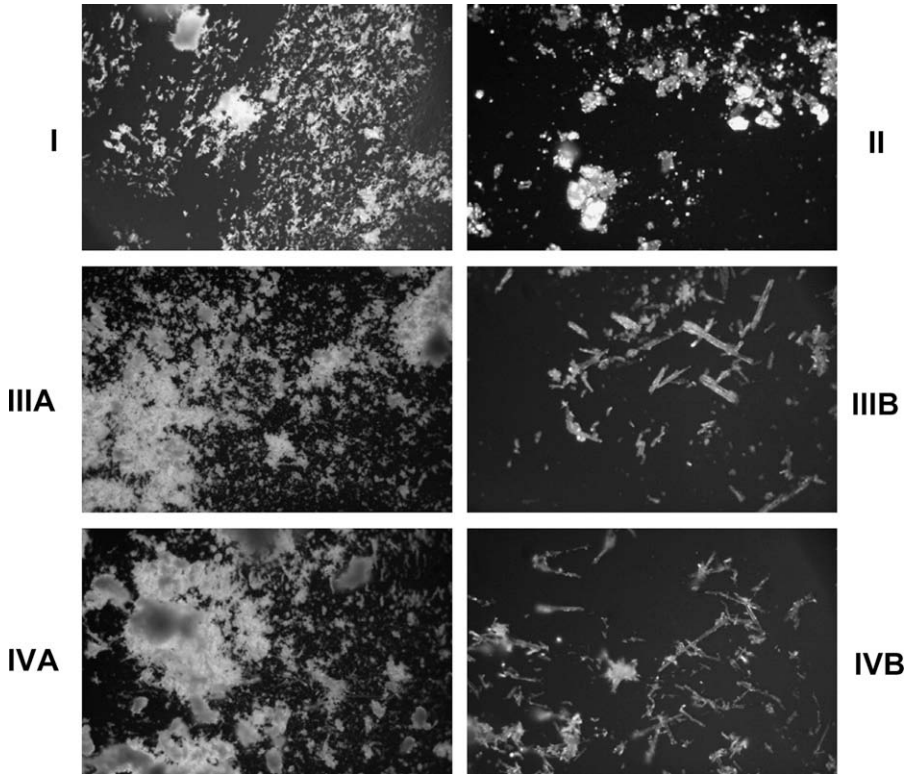

Fig. 3. Photomicrographs of the forms I–IV of Emodepside viewed with plane polarised light. Form III and IV: the batches A and B are presented. The diagonal of the photomicrographs is 1.2 mm.

The onset temperatures and the enthalpies of fusion of the different forms are given in Table 1. Regarding the forms III and IV, IIIB and IVB display higher enthalpies of fusion than IIIA and IVA. A possible explanation might be that the bigger crystals present in IIIB and IVB exhibit less defective sites due to slow crystallisation leading to higher enthalpies of fusion.

As seen in Fig. 2, the amounts of water lost by the forms II–IV are 0.9%, 2.2% and 1.8%. As comparison, a monohydrate would contain 1.6% water. TGA and DSC are not suited to elucidate whether the water is adsorbed to the crystal surface or whether the forms are non-stoichiometric hydrates, since the observed early onset of water evaporation is common in both the cases.

Table 1
Onset temperatures and enthalpies of fusion obtained from the DSC curves of the different forms

	Form I	Form II	Form IIIA	Form IIIB	Form IVA	Form IVB
Onset temperature (°C) [a]	194.4 ± 0.2	178.1 ± 0.6	152.7 ± 0.9	152.9 ± 1.8	138.5 ± 0.1	152.5 ± 0.1
Enthalpy of fusion (J/g)[a,b]	58.6 ± 0.5	44.5 ± 0.6	35.5 ± 1.1	38.9 ± 0.4	31.8 ± 0.4	35.1 ± 0.4

[a] Mean value ± SD (n = 3).
[b] Regarding the forms II–IV, the weight of the samples used to calculate the enthalpy of fusion was corrected to account for the mass loss occurring during the heating due to the evaporation of water. The amount of water sorbed by the respective form at 45% RH (data taken from vapour sorption analysis) was substracted from the weight of the sample.

3.1.2. Hot-stage microscopy

Each form of Emodepside shows birefringence when examined in plane polarised light (Fig. 3). Regarding the forms III and IV, both the batches A and B are presented (see Section 3.1.1). The forms were heated up to 120 °C to investigate whether the loss of water induces any visible changes in the crystals of the forms II–IV. During the heating, crystals of II and IVB were observed to "jump" which can be an indication for dehydration [20]. Although the jumping of the crystals might indicate that the examined crystals are hydrates, the missing of this phenomenon does not rule out the possibility that a hydrate is present. This is valid for the batch IVA as well as for form III. At 120 °C, the interference colours of the different forms are unchanged reflecting that the three-dimensional packing of the crystals of the forms II–IV is not affected by the loss of the water molecules. As this is expected for crystals with water adsorbed to their surfaces as well as for hydrates forming isomorphic dehydrates, this observation does not help to differentiate between hydrate and non-hydrate.

3.2. Spectroscopic analysis and powder X-ray diffraction

The FT-Raman spectra of the four forms show significant differences over the entire range of the spectra (Fig. 4). Differences are also found in the FT-IR spectra (Fig. 5) and in the FT-NIR spectra (Fig. 6), although they are less striking. The differences present in the spectra reflect the variations in the three-dimensional packing of the four forms. Additionally, each form exhibits a unique diffraction pattern when analysed with powder X-ray diffraction (Fig. 7) which further demonstrates the existence of four different crystal forms.

In the FT-IR and FT-NIR spectra of the forms II–IV recorded at ambient conditions, absorption bands of the associated water molecules are visible (Figs. 5 and 6). The FT-NIR spectra (Fig. 6) show intense absorption in the region between 1850 and 2000 nm due to the combination of bending and anti-symmetric stretching modes ($\nu_2 + \nu_3$) of water [21]. In the FT-IR spectra of the forms II–IV (Fig. 5), OH stretching frequencies of water are present in the region of 3700–3400 cm^{-1}. Form III exhibits a single broad OH stretching band centred at approximately 3484 cm^{-1}, whereas the forms II and IV have several overlapping OH stretching bands. The spectrum of form IV further shows a sharp OH stretching band at 3679 cm^{-1}. A broad OH stretching band as visible in the spectrum of form III indicates the presence of water molecules with differing energetic environment [22]. These water molecules can be either adsorbed to the crystal surface [22] or disordered inside the crystal lattice [23]. In contrast to broad OH stretches, a sharp OH stretching band as seen in the spectrum of form IV is indicative of constrained water molecules present in the crystal lattice [23]. Consequently, FT-IR spectroscopy provides indication that form IV is a hydrate.

3.3. Behaviour at different relative humidities

3.3.1. FT-Raman

Varying the RH causes small but reproducible changes in the Raman spectra of the forms II–IV, especially in the C-H stretching

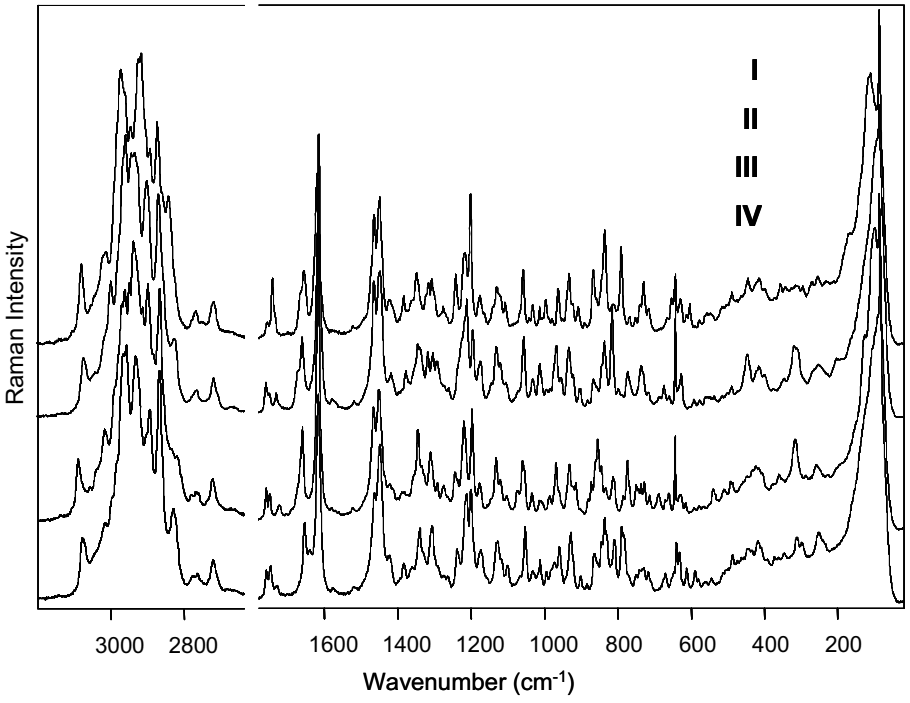

Fig. 4. The FT-Raman spectra of the forms I–IV of Emodepside recorded at ambient conditions.

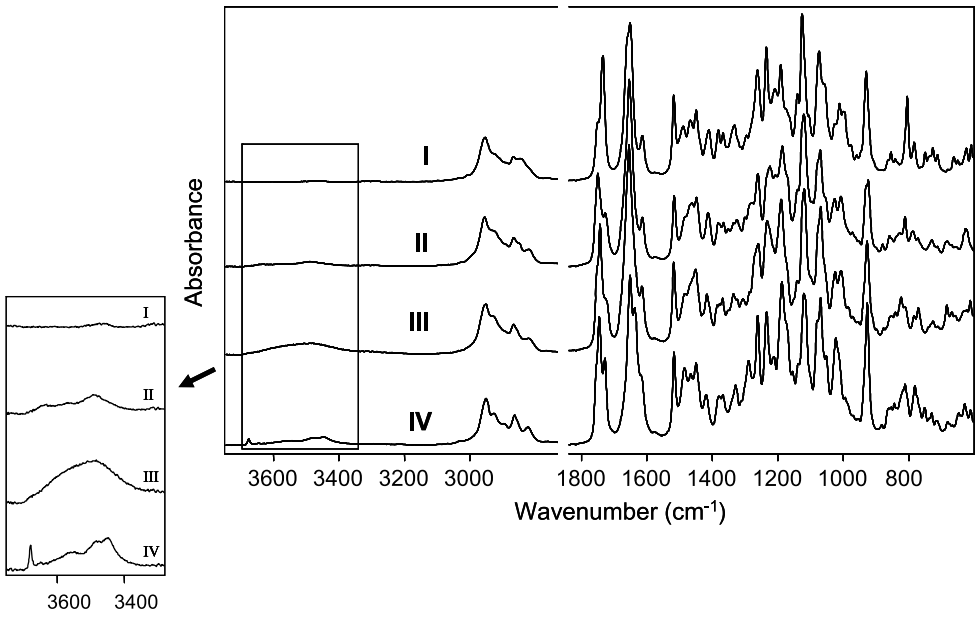

Fig. 5. The FT-IR spectra of the forms I–IV of Emodepside obtained at ambient conditions.

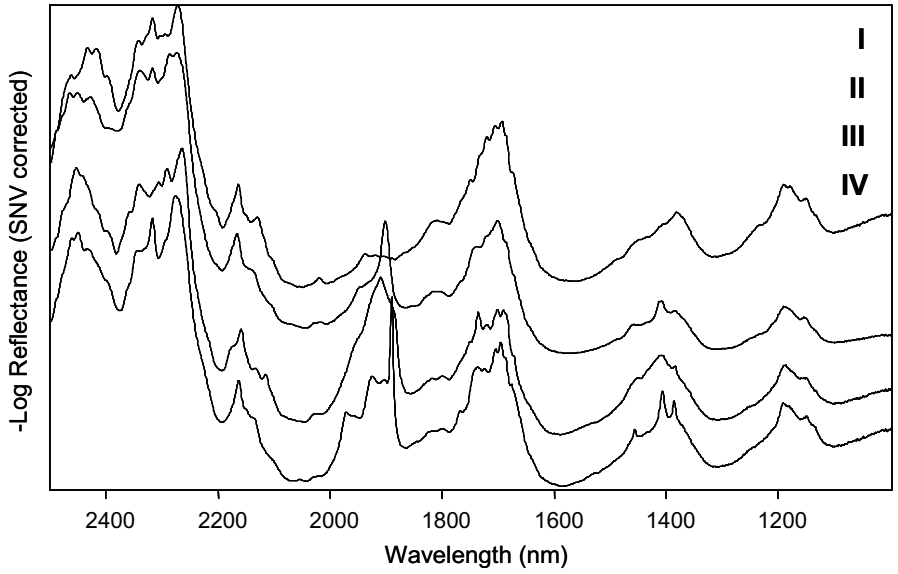

Fig. 6. The FT-NIR spectra (treated with SNV) of the forms I–IV of Emodepside at ambient conditions.

region (3000–2850 cm^{-1}) and in the C=O stretching region (1690–1630 cm^{-1}) (Fig. 8). Form I has identical Raman patterns at the different RH. Regarding the forms III and IV, changes are pronounced when rising the RH from 0% to ambient humidity (45% RH ± 15%). Both forms show shifts in intensity and position of bands in the C—H stretching region. In the C=O stretching region of form IV, the band visible as shoulder of the band at 1654 cm^{-1} at 0% RH is absent at ambient humidity, in addition the intensity of the band at 1654 cm^{-1} has decreased. In exchange, a band at 1639 cm^{-1} emerges at 45% RH. In the C=O stretching region of form III, the two bands present at 0% RH at 1687 cm^{-1} and 1673 cm^{-1} are shifted underneath the C=O vibration band at 1657 cm^{-1} at 45% RH causing a broadening and an increase in the intensity of this band. Consequently, both forms exhibit a shift of C=O stretches towards lower wavenumbers when raising the RH from 0% to ambient humidity. When the RH is changed from ambient humidity to 85%, the spectra of both forms show only minor if any changes at all in the C—H stretching region. In the carbonyl stretching region, a further shift towards lower wavenumbers is observed however being less striking compared to the changes occurring when raising the RH from 0% to 45%. In contrast to the forms III and IV, variation of RH causes only little if any alterations in the C—H stretching region of form II. In the C=O stretching region, the intensity of the band at 1669 cm^{-1} diminishes with rising RH, whereas the band at 1657 cm^{-1} broadens towards lower wavenumbers. Consequently, form II also displays shifts of C=O vibrations towards higher wavelengths.

The changes observed in the Raman spectra of the forms II–IV with varying RH are caused by the absence (0% RH), respectively, the presence (45% and 85% RH) of water. As Raman spectra are sensitive to changes in the local environment inside the crystal lattice [24], the measurements reveal that water molecules are increasingly incorporated into the crystal lattice with rising RH. Consequently, the forms II–IV represent non-stoichiometric hydrates.

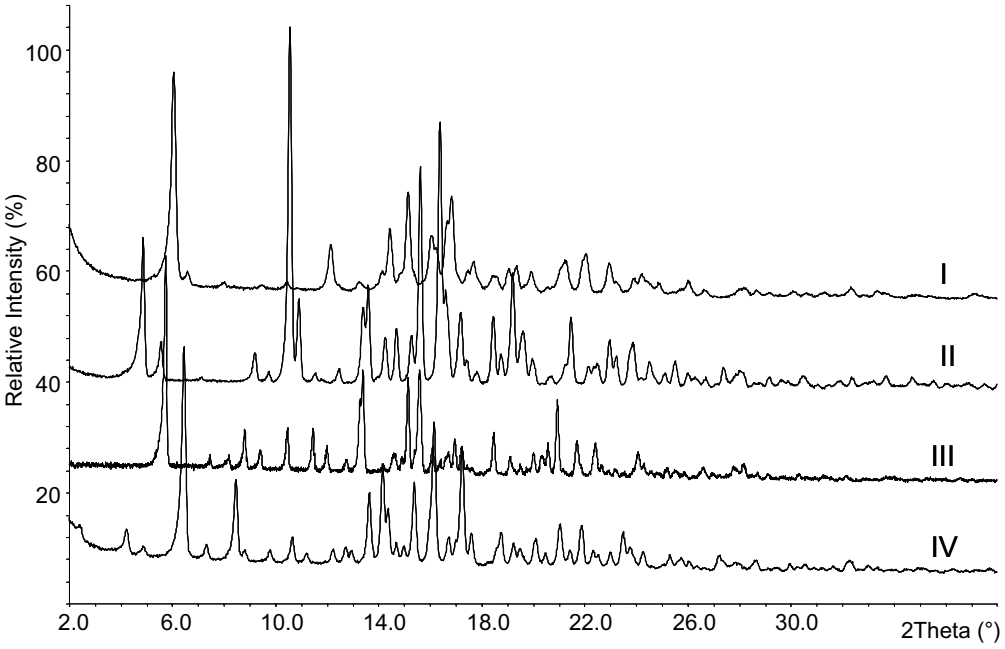

Fig. 7. The PXRD patterns of the forms I–IV of Emodepside recorded at ambient conditions.

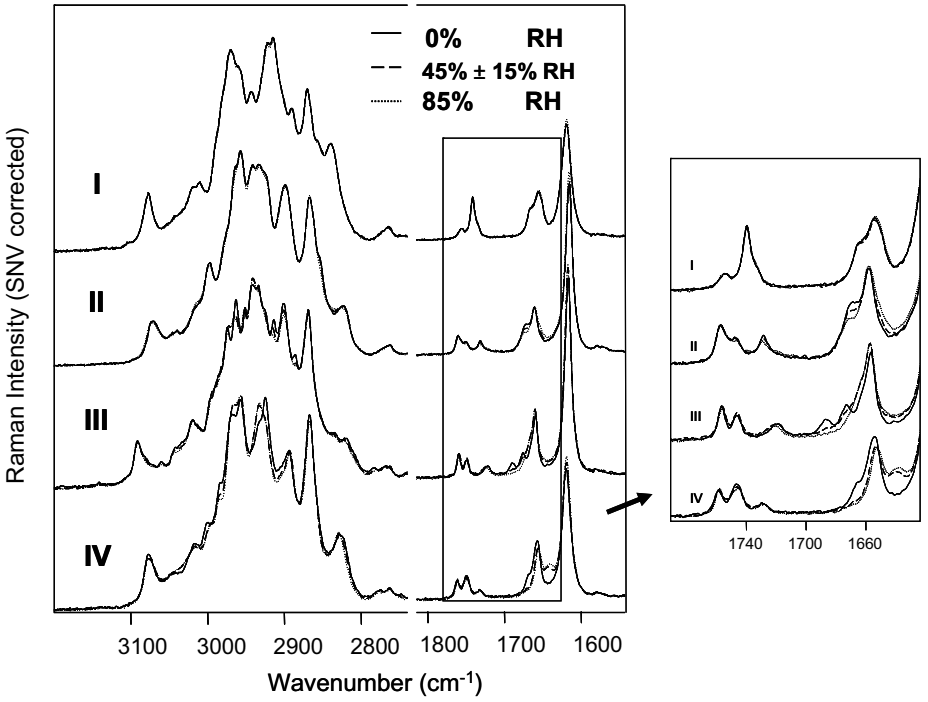

Fig. 8. The FT-Raman spectra (the C—H and C═O stretching regions) of the forms I–IV of Emodepside at different RH. The spectra are normalised using SNV.

The spectra recorded at 0% RH reflect the spectra of the isomorphic dehydrates. With rising RH, water molecules increasingly enter the lattice and interact with carbonyl groups via hydrogen bonding which leads to the observed shift of C═O stretches towards lower wavenumbers. Regarding the forms III and IV, the water molecules also affect C—H vibrations which is either due to direct interaction via van-der-Waals interaction or due to slight reorientations of the C—H groups caused by the presence of water molecules.

The described changes in the C═O stretching region fall into the C═O stretching region of amide groups. However, Raman measurements do not reveal which of the amide groups of Emodepside interact with water molecules in the different forms as the presence of four amide groups in Emodepside (Fig. 1) makes assignment of bands difficult. Additionally, it is difficult to determine whether the C═O stretching bands belonging to the four ester groups of Emodepside (present between 1760 and 1720 cm^{-1}) are also affected by the water molecules due to the low absolute intensity of the bands.

3.3.2. Sorption isotherms

The sorption and desorption curves of the various forms of Emodepside are presented in Fig. 9. The isotherms of the forms dif-

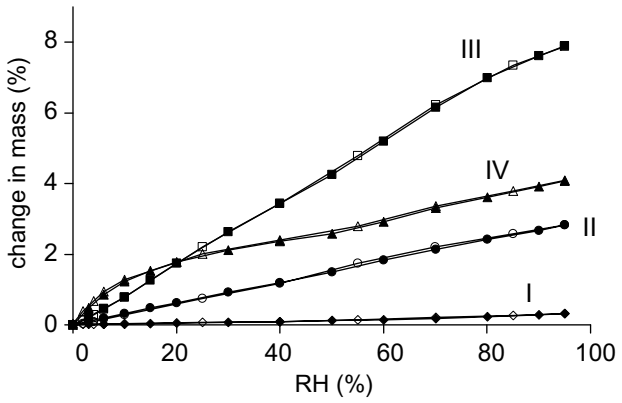

Fig. 9. The water vapour sorption and desorption isotherms of the forms I–IV of Emodepside at 22 °C. The symbols coloured in black represent the data points of the sorption isotherms, whereas the symbols without fillings display the data points of the desorption isotherms.

fer in the amount of the water sorbed and in the shape of the curves. As expected, form I only sorbs minor quantities of water (0.3% = 0.2 mol of water per mole of anhydrous Emodepside from 0% RH to 95% RH) which were not detectable with thermal or spectral analysis. On the other hand, form II takes up 2.8% water (=1.8 mol of water per mole of Emodepside from 0% RH to 95% RH), form III 7.9% (=5 mol of water) and form IV 4.1% (=2.6 mol of water).

Regarding the forms III and IV, the amounts of water sorbed at ambient humidity (in the range of 30% RH–60% RH) are higher than the mass losses of the forms seen in the TG curves (form III: 2.6–5.2% sorbed at 30–60% RH vs. a mass loss of 2.2%, form IV: 2.1–2.9% sorbed vs. a mass loss of 1.8%). The reason is probably that the onset of dehydration is missed with TGA as dehydration starts as soon as the sample is placed on to the balance being exposed to the nitrogen stream.

A common feature of the isotherms of the forms II–IV is that the desorption curve virtually superimposes the sorption curve (Fig. 9). Such behaviour is found in non-stoichiometric hydrates [11] as well as in solids that adsorb water on the crystal surface [25]. However, since it is unlikely that several moles of water (per mole of anhydrous Emodepside) are adsorbed on the crystal surface [26], the virtual superimposition of sorption and desorption curves supports the results obtained from Raman analysis. Concerning the shapes of the curves, the isotherm of form IV differs from the others in the region of low RH. The slope of the sorption curve of form IV being steep from 0% RH to 6% RH flattens between 6% RH and 20% RH. According to Authelin [7] who has linked the degree of order of the water molecules in non-stoichiometric hydrates to the shape of the sorption isotherm, such a change of the slope of the isotherm in the region of low RH indicates the presence of localised water molecules (type I isotherm) or of water molecules with at least some degree of order (type II isotherm). Consequently, the isotherm of form IV provides indication on how the water molecules are bound at low RH. In contrast, the shape of the isotherm of the forms II and III (virtually a straight line) does not well agree with any of the isotherm types described by Authelin. Thus, it does not give any information on the degree of order of the water molecules in the forms II and III.

3.3.3. FT-NIR

The spectra of the different forms at different RH are presented in Fig. 10. At 0% RH the FT-NIR spectra of the isomorphic dehydrates of the forms II–IV are recorded. With rising RH, absorption increases in the spectra of the forms II–IV around 1420 nm due to the combination of symmetric and anti-symmetric stretching modes of water ($\nu_1 + \nu_3$, overtone band) as well as around 1920 nm due to the combination of $\nu_2 + \nu_3$ (OH combination band).

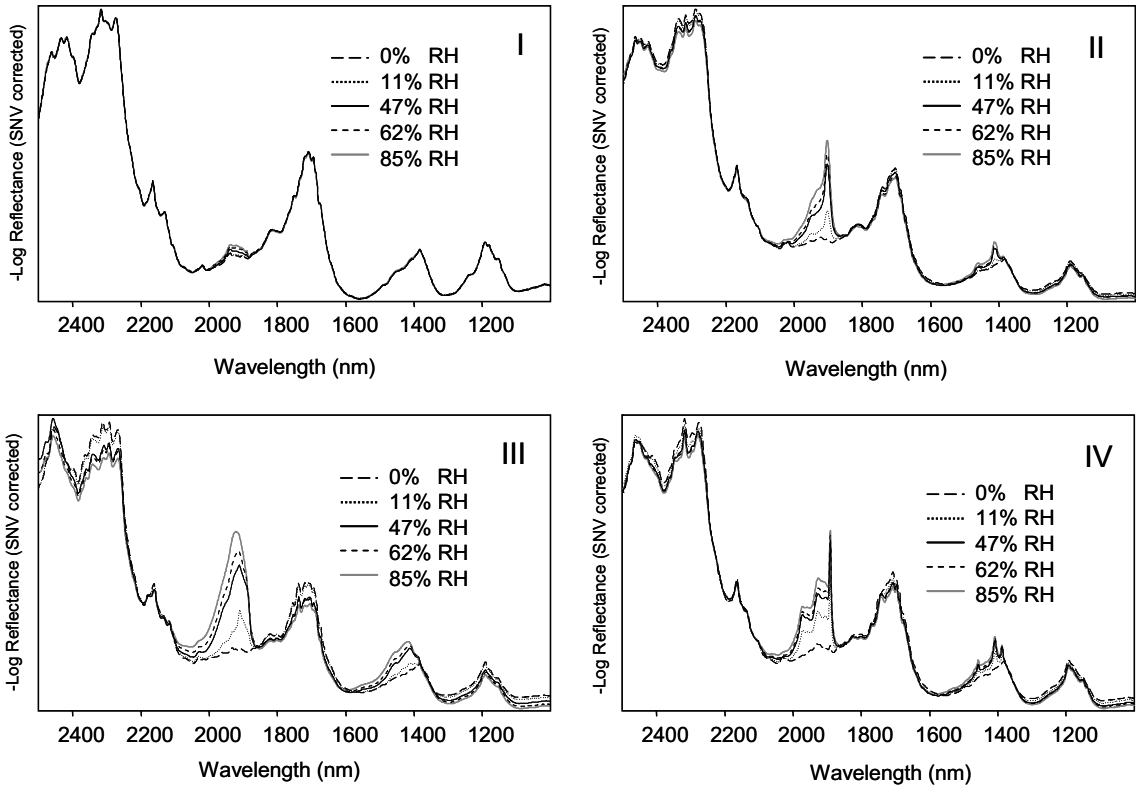

Fig. 10. The FT-NIR spectra (treated with SNV) of the forms I–IV of Emodepside at different RH.

In the spectrum of form I which sorbs minor quantities of water with rising RH, spectral variations are only visible around 1920 nm because of the increased molar absorptivity of water in this wavelength region.

In the overtone region and the OH combination region of the spectra of the forms II–IV, several overlapping bands are visible above 0% RH. This suggests the presence of differently bound water molecules inside the crystal lattices (different "types of water"), as the wavelengths at which water absorbs change with alterations in the strength of hydrogen bonding [17,21,27]. To study the different types of water, the second derivative of the spectral data in the OH combination region was used (Fig. 11) [28,29]. The second derivative has the benefit of enhancing the visual resolution, but it causes the loss of the original shape of the spectra [30]. In the second derivative spectra, the band maxima of the original spectra appear as band minima of negative bands. Fig. 11 shows the second derivative spectra of the forms I–IV at different RH. Regarding the forms II–IV, several negative bands emerge above 0% RH. These negative bands correspond to the OH combination bands in the original spectra. Each negative band represents a certain type of water molecules. The greater the wavelength the band minimum is located at is the stronger is the hydrogen bonding of the water molecules represented by this band [31]. At 11% RH, form II shows two negative bands (at 1903 and 1952 nm). The intensities of these bands increase up to 47% RH (band around 1952 nm) and 85% RH (band at 1903 nm), respectively. This indicates that the amount of the water molecules belonging to the water types reflected by these two bands increases inside the crystal lattice up to the mentioned RH. At 47% RH, a third type of energetically equivalent water molecules arises (negative band at 1935 nm) and the amount of this species of water molecules increases up to high RH.

Form III also shows two types of water at 11% RH (1884 and 1910 nm) (Fig. 11). With rising RH, however, the intensities of the negative bands at 1884 and 1910 nm decrease indicating a diminution of the amount of these types of water molecules. In exchange, stronger hydrogen bonded water molecules appear at 47% RH (negative bands at 1891, 1924, 1954 and 1959 nm). The amount of the water molecules reflected by the bands at 1891 nm and around 1924 nm increases up to 85% RH. The observed changes in band positions and intensities with rising RH might be explained by an increase in the hydrogen bonding of the water molecules by their interaction with the water molecules that additionally enter the crystal lattice.

Regarding form IV, the sharp band at 1891 nm in the raw spectrum produces a sharp and intense negative band in the second derivate spectrum (Fig. 11) which eclipses the intensity changes in the region of 1900–2000 nm. Therefore, this region is zoomed to be able to identify all the bands present. Fig. 11 reveals five types of water incorporated into the crystal lattice of form IV at 11% RH (negative bands at 1891, 1905, 1929, 1959 and 1973 nm). While the intensity of the band at 1929 nm does not change with rising RH, the bands at 1959 nm and 1973 nm increase up to 47% RH, whereas only the band at 1891 nm rises up to high RH. The band at 1905 nm decreases in intensity with rising RH. The changes of the intensities of the bands suggest that the majority of the water molecules are incorporated at low RH. This agrees well with vapour sorption analysis.

In contrast to the forms II–IV, form I shows a single negative band at 1890 nm that increases slightly in intensity with raising RH. The wavelength the band minimum is located at and the low absolute intensity of the band are consistent with water being loosely bound to the crystal surface.

3.4. Crystal structure determination of form IV

The crystal data of a single crystal of form IV of Emodepside stored at ambient humidity are given in Table 2. The results of

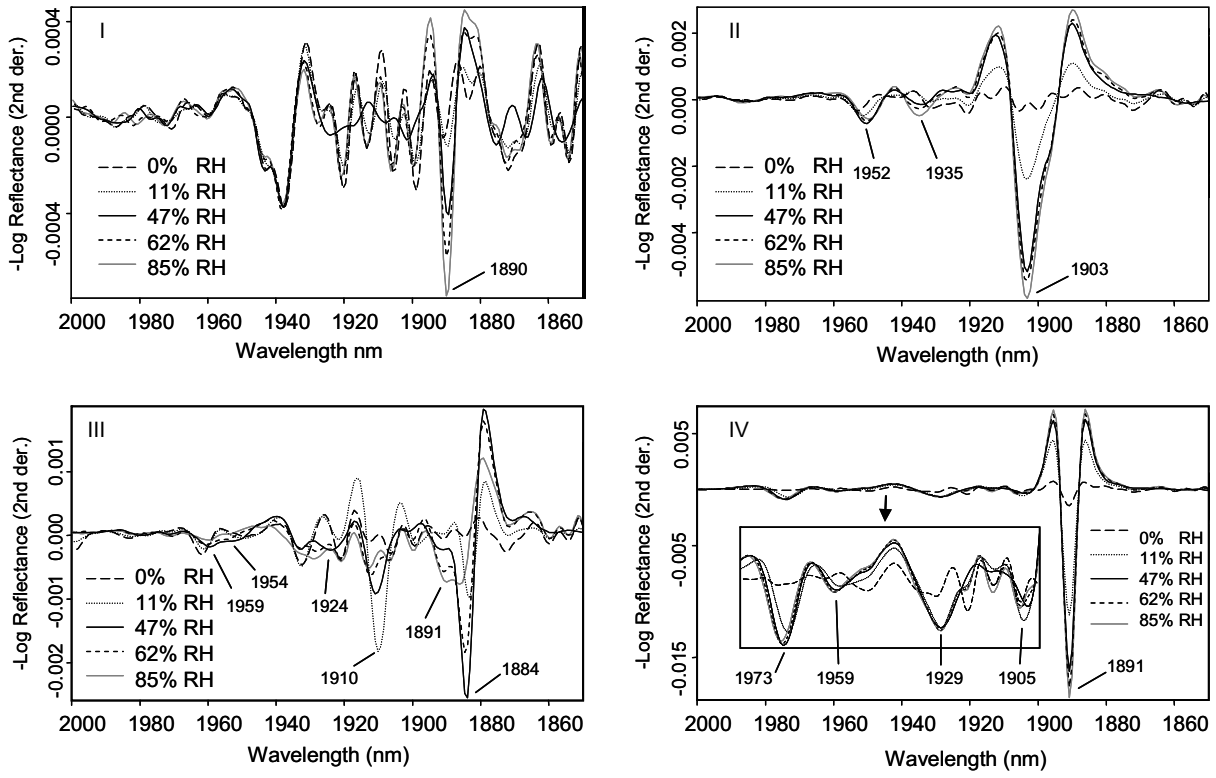

Fig. 11. The FT-NIR spectra (second derivative) of the forms I–IV of Emodepside in the range of 2000–1850 nm obtained at different RH.

Table 2
Crystal data for Emodepside form IV

	Emodepside form IV
Empirical formula	C60 H90 N6 O15.73
Formula weight	1146.98
Temperature (K)	100
Crystal size (mm^3)	0.60 × 0.04 × 0.04
Crystal system	Trigonal
Space group	*P*3
a (Å), *α*(°)	41.1838(3), 90
b (Å), *β*(°)	41.1838(3), 90
c (Å), *γ*(°)	6.48470(10), 120
Volume ($Å^3$)	9525.18(18)
Z	6
Density (calculated) (g/m^3)	1.200
Goodness-of-fit on F^2	1.089
Final *R* indices [*I*>2sigma(*I*)]	R_1 = 0.0403, wR_2 = 0.0974
R indices (all data)	R_1 = 0.0430, wR_2 = 0.0990

the crystal structure determination will be deposited at the Cambridge Structural Database (CSD). Form IV crystallises as twin (twinning by merohedry). Fig. 12 shows that form IV represents a hydrate having two Emodepside molecules and four well-defined positions for water in the asymmetric unit. The sites of the water molecules O1W and O2W are fully occupied, whereas the positions of the water molecules O3W and O4W are occupied to approximately 75% and 70%, respectively. This gives a ratio of 1.7 mol water to 1 mol Emodepside which is found in form IV at 54% RH (see Section 3.3.2). O1W, O3W and O4W are each located in the vicinity of the oxygen atom of an amide group with an O—O distance <3 Å which suggests the formation of hydrogen bonds (Fig. 12). O1W and O4W have similar O—O distances (O1W—O14B: 2.874 Å, O4W—O14A: 2.859 Å), whereas O3W displays a bigger O—O distance (O3W—O7A: 2.994 Å) suggesting that O3W is comparatively weakly hydrogen bonded. In the environment of O2W, the oxygen atoms of two amide groups display O2W—O distances <3 Å (O2W—O7B: 2.959 Å, O2W—O9B: 2.982 Å) which indicates that O2W has two relatively weak hydrogen bonds.

As form IV was found to be a non-stoichiometric hydrate forming an isomorphic dehydrate, the water molecules have to be able to enter/leave the crystal lattice without disrupting the crystal structure. The unit cell (Fig. 13) shows that the water molecules are isolated being located in different structural voids. These voids do not form a straight channel through which the water molecules could easily escape. Therefore, it is difficult to predict how the water molecules leave the crystal.

The results of the crystal structure determination are consistent with the conclusions drawn from Raman analysis and vapour sorption analysis. Raman measurements at different RH suggested form IV to be a hydrate with water molecules hydrogen bonded to C=O groups of amid functions. The shape of the sorption isotherm of form IV (the change of the slope of the isotherm in the region of low RH) indicated the presence of localised water molecules in the crystal lattice at low RH. Regarding NIR analysis, the spectra of form IV at varying RH revealed differently bound water molecules to be present inside the crystal lattice. Having four different water positions in the asymmetric unit, four different bands might be expected in the OH combination region at 54% RH. However, five bands were visible in the spectra at 47% RH and 62% RH (Fig. 11). A possible explanation might be that one of the singly hydrogen bonded water molecules O1W, O3W or O4W exists in two different energetic states due to two possible orientations of the non hydrogen bonded hydrogen atom.

Although the crystal structure of form III is not known, the results of the various measurements indicate the presence of large channels in the crystal structure. This conclusion was drawn because of the following results: form III incorporates the highest amount of water molecules. Dehydration is not accompanied by a jumping of the crystals indicating that the water molecules can very easily leave the crystal structure. The strength of the bonding of the water molecules incorporated into the crystal lattice rises

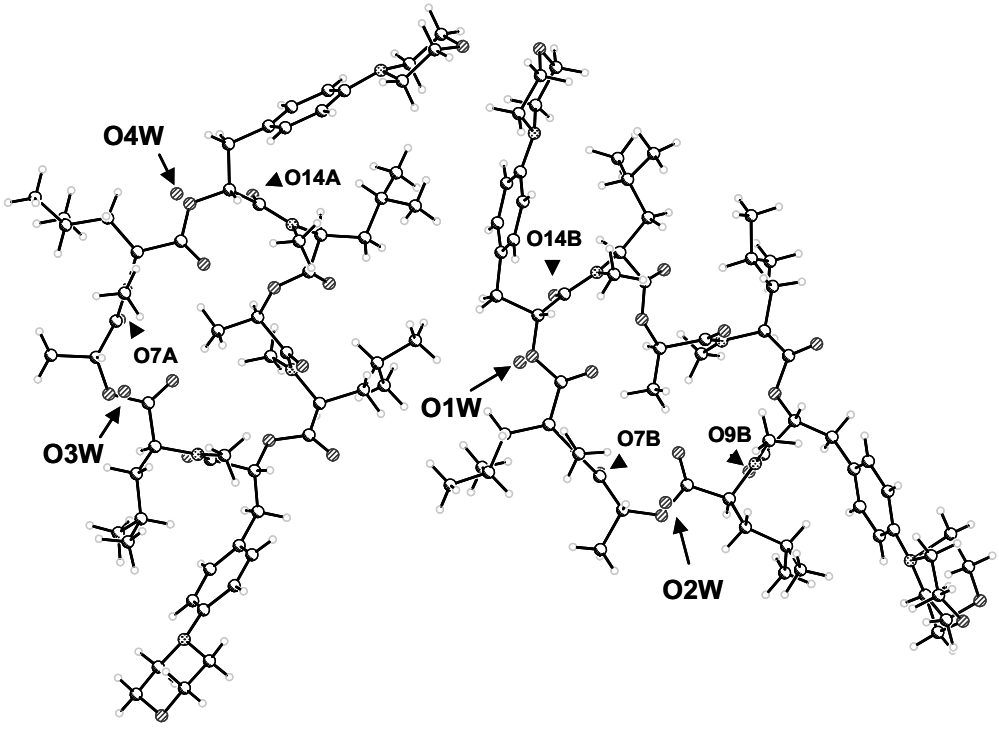

Fig. 12. The asymmetric unit of form IV of Emodepside found at ambient conditions. Labelled: the oxygen atoms representing the four water molecules O1W, O2W, O3W and O4W and the adjacent oxygen atoms of the two Emodepside molecules (O—O distance <3 Å).

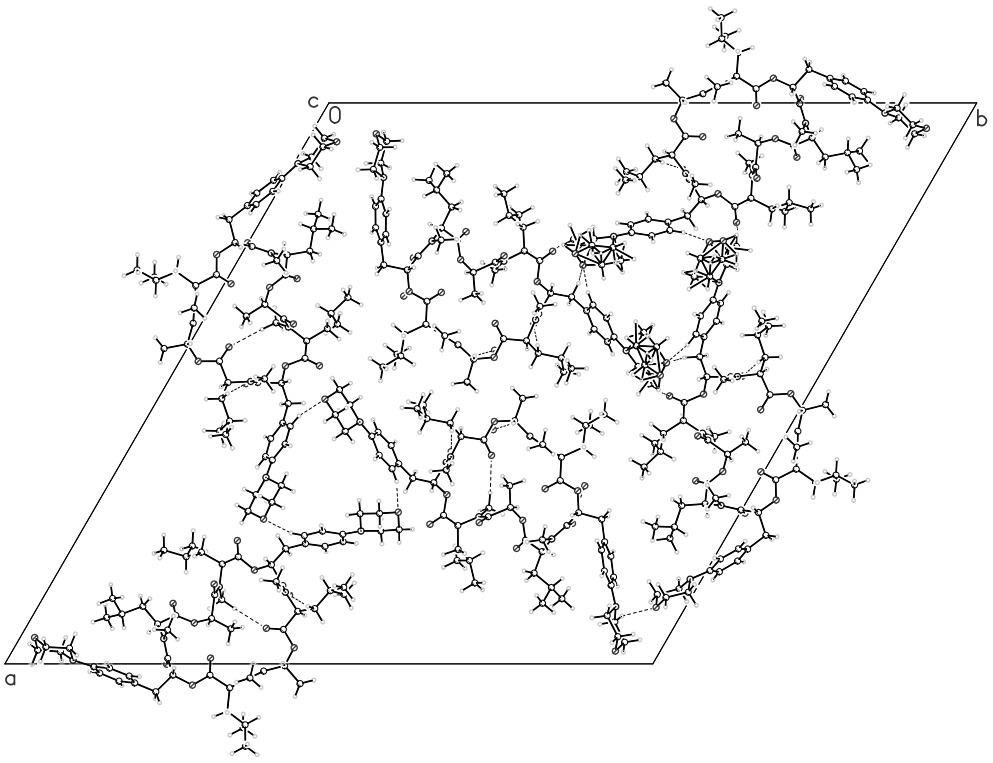

Fig. 13. The unit cell of form IV of Emodepside at ambient conditions viewed down the *c* axis.

with increasing RH suggesting the interaction with the water molecules which enter the lattice. The water molecules not only affect the vibration of C=O groups, but also of C—H groups.

4. Conclusions

The analysis of the behaviour of the forms II–IV of Emodepside at different RH using FT-Raman and FT-NIR spectroscopy and vapour sorption/desorption analysis revealed that all three forms represent non-stoichiometric hydrates with differently bound water molecules inside the crystal lattice. Regarding form IV, results were confirmed by crystal structure determination. While Raman analysis served as an indirect proof that the water molecules are incorporated into the crystal lattices, NIR spectroscopy was suitable to differentiate between different types of water molecules present inside the crystal lattices. Vapour sorption analysis provided information on the order of the water molecules incorporated into the crystal lattice of form IV. Consequently, the methods employed were not only able to elucidate that all three forms are hydrates, but they also highlighted the differences between the three non-stoichiometric hydrates allowing some conclusions concerning the way the water molecules are incorporated into the crystal lattices.

References

[1] A.C. Schmidt, I. Schwarz, Solid-state characterization of non-stoichiometric hydrates of ester-type local anaesthetics. Part XI. Crystal polymorphism of local anaesthetic drugs, Int. J. Pharm. 320 (2006) 4–13.
[2] J. Han, R. Suryanarayanan, A method for the rapid evaluation of the physical stability of pharmaceutical hydrates, Thermochim. Acta 329 (1999) 163–170.
[3] H. Zhu, P. Varlashkin, S. Long, C. Kidd, Dehydration, Hydration Behavior, and Structural Analysis of Fenoprofen Calcium, J. Pharm. Sci. 90 (2001) 845–859.
[4] A.M. Amado, M.M. Nolasco, P.J.A. Ribeiro-Clar, Probing pseudopolymorphic transitions in pharmaceutical solids using Raman spectroscopy: hydration and dehydration of theophylline, J. Pharm. Sci. 96 (2007) 1366–1379.
[5] R.K. Khankari, D.J.W. Grant, Pharmaceutical hydrates, Thermochim. Acta 248 (1995) 61–79.
[6] U.J. Griesser, The importance of solvates, in: R. Hilfiker (Ed.), Polymorphism in the Pharmaceutical Industry, VILEY-VCH Verlag GmbH & Co. KGaA, Weinheim, Germany, 2006, pp. 211–233.
[7] J.-R. Authelin, Thermodynamics of non-stoichiometric pharmaceutical hydrates, Int. J. Pharm. 303 (2005) 37–53.
[8] S.R. Vippagunta, H.G. Brittain, D.J.W. Grant, Crystalline solids, Adv. Drug Deliv. Rev. 48 (2001) 3–26.
[9] L.T. Ruth, U.J. Griesser, K.R. Morris, S.R. Byrn, J.G. Stowell, X-ray diffraction and solid-state NMR investigation of the single-crystal to single-crystal dehydration of thiamine hydrochloride monohydrate, Cryst. Growth Des. 3 (2003) 997–1004.
[10] G.A. Stephenson, B.A. Diseroad, Structural relationship and desolvation behavior of cromolyn, cefazolin and fenoprofen sodium hydrates, Int. J. Pharm. 198 (2000) 167–177.
[11] G.A. Stephenson, E.G. Groleau, R.L. Kleemann, W. Xu, D.R. Rigsbee, Formation of isomorphic desolvates: creating a molecular vacuum, J. Pharm. Sci. 87 (1998) 536–542.
[12] S. Petit, G. Coquerel, Mechanism of several solid-solid transformations between dihydrated and anhydrous copper(II) 8-hydroxyquinolinates. Proposition for a unified model for the dehydration of molecular crystals, Chem. Mater. 8 (1996) 2247–2258.
[13] J.M. Rollinger, A. Burger, Physico-chemical characterization of hydrated and anhydrous crystal forms of amlodipine besylate, J. Therm. Anal. Calorim. 68 (2002) 361–372.
[14] S.M. Reutzel-Edens, A.W. Newman, Physical characterization of hygroscopicity in pharmaceutical solids, in: R. Hilfiker (Ed.), Polymorphism in the Pharmaceutical Industry, WILEY-VCH Verlag GmbH & Co. KGaA, Weinheim, Germany, 2006, pp. 235–258.
[15] G.A. Stephenson, J.G. Stowell, P.H. Toma, R.R. Pfeiffer, S.R. Byrn, Solid-state investigations of erythromycin A dihydrate: structure, NMR spectroscopy, and hygroscopicity, J. Pharm. Sci. 86 (1997) 1239–1244.
[16] I. Miroshnyk, L. Khriachtchev, S. Mirza, J. Rantanen, J. Heinämäki, J. Yliruusi, Insight into thermally induced phase transformations of erythromycin A dihydrate, Cryst. Growth Des. 6 (2006) 369–374.
[17] J.P. Higgins, S.M. Arrivo, R.A. Reed, Approach to the determination of hydrate form conversions of drug compounds and solid dosage forms by near-infrared spectroscopy, J. Pharm. Sci. 92 (2003) 2303–2316.
[18] G.A. Stephenson, R.A. Forbes, S.M. Reutzel-Edens, Characterization of the solid state: quantitative issues, Adv. Drug Deliv. Rev. 48 (2001) 67–90.
[19] G.M. Sheldrick, A short history of SHELX, Acta Crystallogr. A64 (2008) 112–122.
[20] A. Kofler, Thermomikro-Methoden zur Kennzeichnung organischer Stoffe und Stoffgemische, Verlag Chemie Weinheim, Germany, 1954, pp. 28–32.
[21] H. Maeda, Y. Ozaki, M. Tanaka, N. Hayashi, T. Kojima, Near infrared spectroscopy and chemometrics studies of temperature-dependent spectral

variations of water: relationship between spectral changes and hydrogen bonds, J. Near Infrared Spectrosc. 3 (1995) 191–201.
[22] K.R. Morris, Structural aspects of hydrates and solvates, in: H.G. Brittain (Ed.), Polymorphism in Pharmaceutical Solids, Marcel Dekker AG, Basel, Switzerland, 1999, pp. 125–181.
[23] N. Redman-Furey, M. Dicks, A. Bigalow-Kern, R.T. Cambron, G. Lubey, C. Lester, D. Vaughn, Structural and analytical characterization of three hydrates and an anhydrate form of risedronate, J. Pharm. Sci. 94 (2005) 893–911.
[24] A.D. Gift, L.S. Taylor, Hyphenation of Raman spectroscopy with gravimetric analysis to interrogate water-solid interactions in pharmaceutical systems, J. Pharm. Biomed. Anal. 43 (2007) 14–23.
[25] K. Umprayn, R.W. Mendes, Hygroscopicity and moisture adsorption kinetics of pharmaceutical solids: a review, Drug Dev. Ind. Pharm. 13 (1987) 653–693.
[26] M.J. Kontny, G. Zografi, Sorption of water by solids, in: H.G. Brittain (Ed.), Physical Characterization of Pharmaceutical Solids, Marcel Dekker AG, Basel, Switzerland, 1995, pp. 387–418.
[27] M. Blanco, J. Coello, H. Iturriaga, S. Maspoch, C. de la Pezuela, Near-infrared spectroscopy in the pharmaceutical industry, Analyst 123 (1998) 135R–150R.
[28] E. Räsänen, J. Rantanen, A.C. Jorgensen, M. Karjalainen, T. Paakkari, J. Yliruusi, Novel identification of pseudopolymorphic changes of theophylline during wet granulation using near infrared spectroscopy, J. Pharm. Sci. 90 (2001) 389–396.
[29] K.L. Vora, G. Buckton, D. Clapham, The use of dynamic vapour sorption and near infra-red spectroscopy (DVS–NIR) to study the crystal transitions of theophylline and the report of a new solid-state transition, Eur. J. Pharm. Sci. 22 (2004) 97–105.
[30] H.M. Heise, R. Winzen, Chemometrics in near-infrared spectroscopy, in: H.W. Siesler, Y. Ozaki, S. Kawata, H.M. Heise (Eds.), Near-Infrared Spectroscopy, Principles, Instruments, Applications, WILEY-VCH Verlag GmbH & Co KGaA, Weinheim, Germany, 2002, pp. 147–149.
[31] V. Fornés, J. Chaussidon, An interpretation of the evolution with temperature of the $\nu_2+\nu_3$ combination band in water, J. Chem. Phys. 68 (1978) 4667–4671.